Earth Planet. Sci. Lett. 648 (2024) 119071

Contents lists available at ScienceDirect

Earth and Planetary Science Letters

journal homepage: www.elsevier.com/locate/epsl

# Earth's hypsometry and what it tells us about global sea level

V.K. Pedersen [*,a], N. Gomez [b], J.X. Mitrovica [c], G. Jungdal-Olesen [a], J.L. Andersen [a], J. Garbe [d,e], A. Aschwanden [f], R. Winkelmann [d,e]

[a] Department of Geoscience, Aarhus University, Aarhus, Denmark
[b] Department of Earth and Planetary Sciences, McGill University, Montreal, Canada
[c] Department of Earth and Planetary Sciences, Harvard University, USA
[d] Potsdam Institute for Climate Impact Research (PIK), Member of the Leibniz Association, Potsdam, Germany
[e] Institute of Physics and Astronomy, University of Potsdam, Potsdam, Germany
[f] Geophysical Institute, University of Alaska Fairbanks, Fairbanks, USA

ARTICLE INFO

*Keywords:*
Global topography
Hypsometry
Global mean sea level

ABSTRACT

Over geological time scales, the combination of solid-Earth deformation and climate-dependent surface processes have resulted in a distinct hypsometry (distribution of surface area with elevation) on Earth, with the highest concentration of surface area focused near the present-day sea surface. However, in addition to a single, well-defined maximum at the present-day sea surface, Earth's hypsometry is also characterized by a prominent maximum ~2–5 m above this level, with the range accounting for uncertainties in recent digital elevation models. Here we explore the nature of this enigmatic maximum and examine, using a gravitationally self-consistent model of ice-age sea-level change, how it evolved over the last glacial cycle and may evolve moving towards a near-ice-free future. We argue that the hypsometric maximum captures topographic conditions at the end of the last deglaciation phase and subsequent glacial isostatic adjustment (GIA) raised it from the sea surface to its present-day elevation. Moreover, ongoing GIA will raise the maximum a further ~2 m in the absence of future ice mass loss. If a portion of the hypsometric maximum has persisted for longer than Holocene time scales, the resulting GIA-converged elevation of the hypsometric maximum at +4–7 m above the sea surface implies a longer-term mean state of the Earth that may reflect lower ice volumes, trends in erosion, dynamic topography, or a combination of these. The signature of these various contributions on present-day hypsometry is intimately connected to the time scale of erosional and depositional processes near shorelines.

## Introduction

Earth's topography is shaped by a complex interplay between solid-Earth processes that deform the Earth from within and surface processes that modify the shape of the Earth at the surface. Over geological time scales, this interplay has resulted in a distinct hypsometric distribution (distribution of surface area with elevation; Fig. 1A-C, black curve). Most of Earth's surface area constitutes ocean (~71% at present), wherein the vast abyssal plains between ~3–6 km depth comprise the larger part. However, the highest concentration of surface area on Earth is focused in a narrow elevation range near the present-day sea surface, which is also where a significant fraction of Earth's population resides.

Previous work on Earth's hypsometry has focused on onshore cumulative surface area and paleo-shorelines on million-year timescales from the middle Jurassic to Miocene age, to infer tectonically driven changes in global sea level and large-scale changes in continental hypsometry on these long (largely ice-free) geological time scales (e.g., Bond, 1978; Harrison et al., 1983; Algeo and Wilkinson, 1991; Rowley, 2017). On shorter (more recent) geological time scales, where the Earth has been dominated by recurring glaciations and accompanying sea-level changes, previous work on Earth's hypsometry has focused on high-elevation hypsometry, finding maxima in hypsometric distributions to correlate with local snowline altitude (e.g., Brozovic et al., 1997; Mitchell and Montgomery, 2006; Egholm et al., 2009; Pedersen et al., 2010). These studies argue for an efficient glacial-buzzsaw erosion mechanism that leaves only a limited amount of topography above the

* Corresponding author.
*E-mail addresses:* vkp@geo.au.dk (V.K. Pedersen), natalya.gomez@mcgill.ca (N. Gomez), jxm@eps.harvard.edu (J.X. Mitrovica), gpo@geo.au.dk (G. Jungdal-Olesen), jane.lund@geo.au.dk (J.L. Andersen), julius.garbe@pik-potsdam.de (J. Garbe), aaschwanden@alaska.edu (A. Aschwanden), ricarda@pik-potsdam.de (R. Winkelmann).

https://doi.org/10.1016/j.epsl.2024.119071
Received 5 April 2024; Received in revised form 9 October 2024; Accepted 10 October 2024

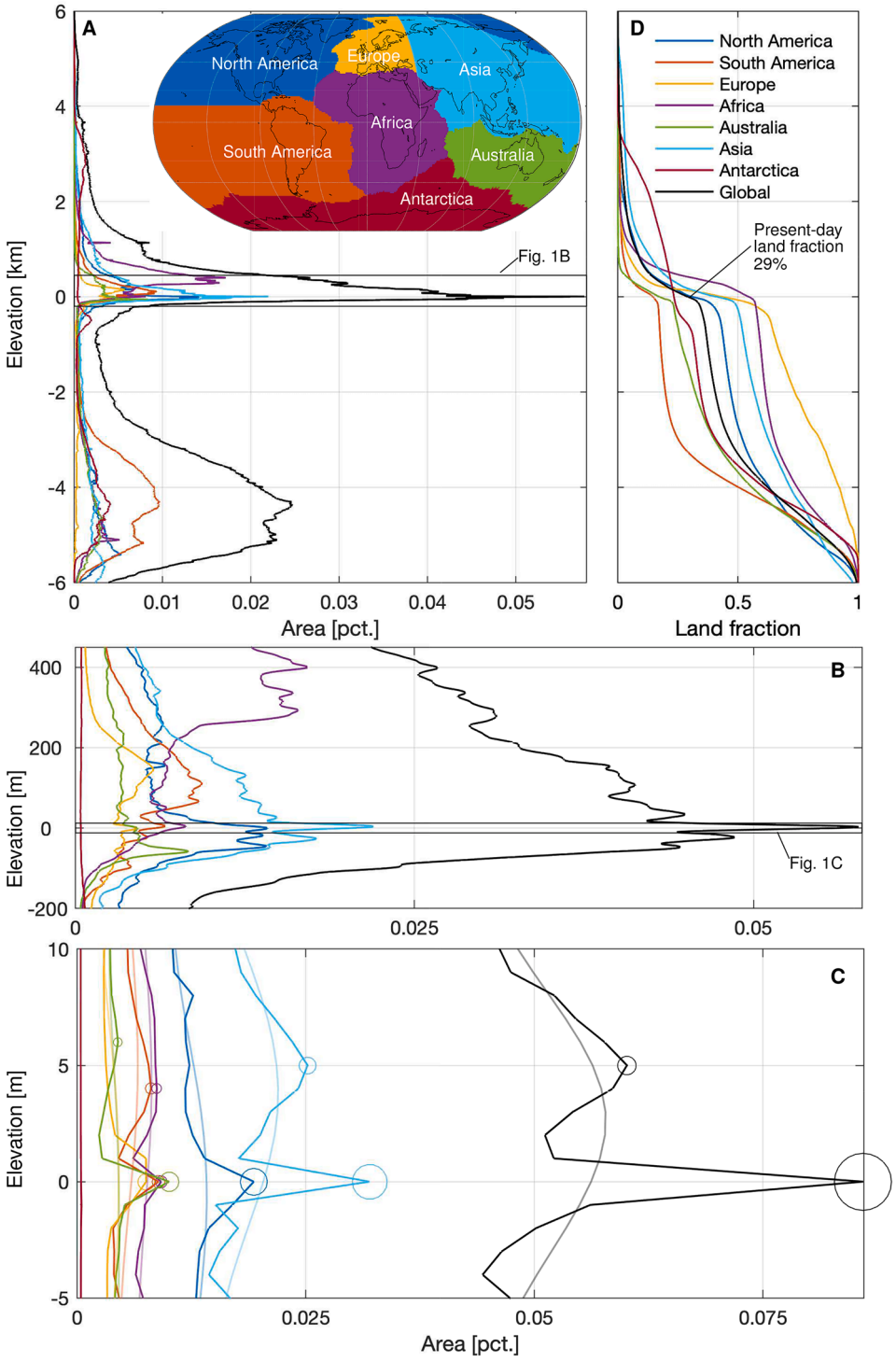


**Fig. 1.** Present-day global hypsometry. A, Hypsometric distributions (distribution of surface area with elevation) for the entire Earth (black curve) and for distinct regions as defined in the inset, for the elevation span between −6 to 6 km (GEBCO Compilation Group, 2023). Legend in D. B-C, A closer look at the hypsometric distributions in the intervals between −200 and 450 m and −5 and 10 m, respectively. Note that in C both the smoothed and the raw (un-smoothed) hypsometric curves are shown, whereas A-B show only smoothed curves. We note that the smoothened global hypsometric curve shows an intermediate hypsometric maximum at ~3 m (merging the 0-m and the 5-m maxima). Circles in C represent peak prominence (findpeaks, The MathWorks Inc., 2023) for significant hypsometric maxima (top 3 within ±50 m from the sea surface) for each continental region and the global curve. D, Normalized cumulative surface area for the entire Earth (black curve) and the different regions (integrating the hypsometric distributions from the highest elevations to the deepest oceans; shown between −6 to 6 km).

local snowline – a glacial erosional base level recognized in hypsometric distributions worldwide (Egholm et al., 2009). However, the ultimate base level on Earth is set by the sea surface that, for most erosive agents, controls the transition between erosion that brings topography down to the sea surface and deposition that fills ocean basins up to the sea surface. Consequently, the largest concentration of surface area on Earth is found near the present sea surface (Fig. 1A-B).

However, on closer inspection, Earth's hypsometry does not constitute a single well-defined maximum at the present-day sea surface (0 m). Instead, Earth's hypsometry constitutes two hypsometric maxima near the present sea surface; a narrow maximum located exactly at 0 m and a second broader maximum located ~5 m above the present sea surface in the GEBCO Compilation Group (2023) digital elevation model (General Bathymetric Chart of the Oceans; GEBCO Compilation Group 2023; Fig. 1C). We note that the 0-m hypsometric maximum has not been a consistent feature in the global GEBCO DEMs (Fig. 2; GEBCO Compilation Group 2021, 2022, 2023), but has appeared with new 'remove and restore' blending procedures implemented since 2022, that aim to reduce edge effects between sparse regional data grids and the global base grid (e.g., Smith and Sandwell, 1997; Becker et al., 2009; Hell and Jakobsson, 2011). The 0-m peak that has appeared with these new procedures arises partly from updated input source data sets and partly through the grid generation process and may be associated with interpolation biases as the GEBCO grid is not based on measured data in all shallower water areas (Global GEBCO Center, personal communication).

The appearance of the 0-m peak has reduced the peak width and prominence of the 5-m peak in the GEBCO DEM (GEBCO Compilation Group, 2021 versus GEBCO Compilation Group, 2023; Fig. S1) according to the definition of these metrics (findpeaks, The MathWorks Inc., 2023), while the surrounding hypsometry has not changed significantly (Fig. 2). We note also that the 'corrected' digital surface model DeltaDTM (global coastal digital terrain model covering 0–10 m a.s.l.), as well as other similar models (Pronk et al., 2024), find the hypsometric maximum to be lower (~2–4 m a.s.l.). Nonetheless, the peak is a significant feature of all DEMs, and while we adopt the GEBCO Compilation Group (2023) DEM in the evolutionary calculations below, we take the range +2–5 m to be a measure of uncertainty in the elevation of the hypsometric maximum. This curious feature of Earth's hypsometry and its origin remains unexplored.

The high concentration of surface area near the present-day sea surface (Fig. 1A-C) makes the global land fraction very sensitive to changes in sea level itself (Fig. 1D). Indeed, any sea-level change will result in an altered land-ocean fraction as dictated by the hypsometric distribution (Bond, 1978), and such a change in land fraction will modulate the conversion from ocean-volume changes to global sea-level changes. Global glacial isostatic adjustment (GIA) sea-level models consider the influence of hypsometry on ocean area inherently when including migrating shorelines and the growth and retreat of marine-based ice sheets (e.g., Mitrovica and Milne, 2003; Milne and Mitrovica, 2008), but it remains challenging to consider these effects in the context of regional ice-sheet modelling studies that explore the contribution of ice sheets to past and future sea level. In particular, the choice of ocean area and corrections related to marine-grounded ice below flotation (e.g., Adhikari et al., 2020; Goelzer et al., 2020) may influence the conversion of ice volume to water-equivalent sea-level changes by several meters at the Last Glacial Maximum (LGM). Likewise, recent work has highlighted the importance of solid-Earth deformation and water expulsion within previously glaciated marine settings for global scale sea-level changes and future sea-level projections (e.g., Gomez et al., 2010, 2024; Pan et al., 2021; Yousefi et al., 2022).

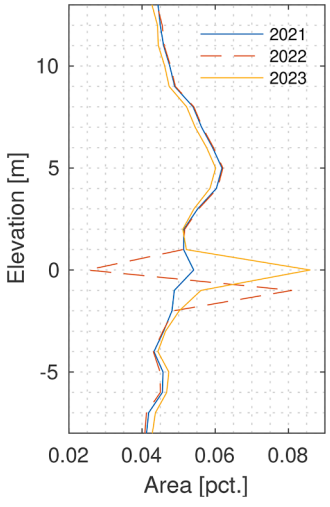


**Fig. 2.** Comparison of global hypsometry for different GEBCO releases (GEBCO Compilation Group 2021, 2022, 2023) near the present-day sea surface (−8 to 13 m).

Here we explore the origin of the hypsometric maximum ~2–5 m above the sea surface by assessing its evolution in time and we consider the effect of Earth's particular hypsometry (formed over millennial- to multi-million-year time scales) on the relationship between coastline evolution and global sea-level changes over the last glacial cycle. Variations in global ice volume resulted in significant global excursions in sea level, modulated regionally by solid-Earth deformation, gravitational effects, and effects from Earth's rotation (e.g., Farrell and Clark, 1976; Mitrovica and Milne, 2003). To examine the behaviour of this hypsometric maximum and the influence of Earth's hypsometry for global sea levels higher than today, we also consider a projection scenario where both the Greenland Ice Sheet (GrIS) and the Antarctic Ice Sheet (AIS) retreat over multi-millennial timescales. We emphasise that this scenario is not meant to represent a realistic future scenario *per se*, but rather an end-member model for Earth's long-term future sea level.

## Methods

### *Global hypsometry and land fraction*

We calculate present-day global hypsometry based on the global GEBCO Compilation Group (2023) DEM including ice (GEBCO Compilation Group, 2023), with a resolution of 15 arc-seconds. The hypsometry is calculated using 1-m elevation bins and is subsequently smoothed using a loess filter over a moving average of 30 m (Fig. 1A-C, black curve). Hypsometry is calculated based on a DEM that includes ice, in part because bedrock elevations in areas of ice cover, notably the Antarctic, are vastly under sampled and uncertain to a level of 100s of meters (Morlighem et al., 2020).

For computational reasons, we calculate global hypsometry for each latitudinal band separately, and iteratively sum up their contributions to arrive at the global curve. The latitudinal dependence on the area of the GEBCO grid is handled using the haversine formula (e.g., Inmann, 1835). Subsequently, we define a normalized curve for cumulative global surface area with elevation (Fig. 1D), integrating the global hypsometry from the top. This curve represents the total land area that exists above any given elevation, corresponding to a land fraction of ~29% at the level of the present-day sea surface. In addition, we calculate hypsometry for seven regions worldwide (Fig. 1A-C). These regions (Fig. 1A, inset) are defined following major tectonic plate boundaries from Bird (2003) and Argus et al. (2011), although we have connected continents with their immediate oceanic regions. Since we focus on features of the hypsometric distributions near the present-day sea surface, this division of the deep ocean basins is of negligible importance. To assess Europe and Asia separately, we split the Eurasian plate in our analyses at longitude 45°E.

To explore Earth's hypsometry over the last glacial cycle and into deep future, we utilize a global, gravitationally self-consistent sea-level model that computes the time-varying deformation of a rotating,

Maxwell viscoelastic Earth model with a depth-dependent Earth structure (e.g., Kendall et al., 2005; Milne and Mitrovica, 1996). The model includes migrating shorelines, the inundation of water into regions previously covered by grounded, marine-based ice, and expulsion of water as grounded ice advances into such settings (Mitrovica and Milne, 2003). The sea-level model is solved using a pseudo-spectral numerical scheme up to spherical harmonic degree and order 256 (Kendall et al., 2005). We adopt, in our standard model, the VM5a Earth model and the corresponding global ICE6G_C ice history (Argus et al., 2014; Peltier et al., 2015) extending from 122 ka until the present (0 BP). The sea level simulation is run from 122 ka until the present, but we treat the first 30 kyr of the model run as a spin-up phase that will not be considered in the interpretation of our results.

For our sea-level projections, we use ice-sheet model predictions from Aschwanden et al. (2019) and Garbe et al. (2020) for Greenland and Antarctica, respectively. The RCP8.5 control simulation of Aschwanden et al. (2019) models the demise of the GrIS over a period of ~1,000 yrs (starting from calendar year 2008). For Antarctica, we use the quasi-static (transient) reference simulation of Garbe et al. (2020) under the assumption that the entire AIS disappears over ~10 kyr, starting from 1950, with most ice loss occurring within the first ~6,000 yrs. The global sea-level simulation is continued for 20 kyr into the future to account for ongoing GIA.

The temporal resolution of the sea-level simulation ranges from 2,000 yrs to 250 yrs in the past (Peltier et al., 2015; Argus et al., 2014), whereas the resolution of the projections is ~30 yrs until the GrIS has dissapeared and ~100 yrs for the remainder of the simulation. We assume ice and water densities of 920 kg $m^{-3}$ and 1,000 kg $m^{-3}$, respectively. We note that our approach does not consider ocean-dynamic or steric sea-level changes.

To examine the evolution of Earth's hypsometry over time, we interpolate our results from the global sea-level simulation onto the global high-resolution GEBCO grid using bilinear interpolation. For every time step we adjust the ice-free version of the present-day GEBCO DEM for global sea-level changes relative to present day and add the global distribution of grounded ice. From these reconstructions of past topography and bathymetry, we calculate global hypsometry in a similar fashion as for the present day. We emphasize that hypsometry is calculated based on the ice surface (bedrock topography + ice thickness) for regions where the ice is grounded. Regions with grounded, marine-based ice will thus contribute to hypsometry above the sea surface whereas regions with floating ice will be considered part of the ocean. This formulation ensures that the negative portion of the hypsometric curve represents the ocean basin only, while regions with grounded marine-based ice are considered part of the land mask. This approach is consistent with the ocean area being bounded either by the coastline or the grounding line in the case of marine-based ice, as is common when estimating sea-level changes (e.g., Adhikari et al., 2020; Goelzer et al., 2020). We track sea-level change near the coastline and global land fraction through time and these will be used to calculate changes in global mean sea level (GMSL).

In addition to this standard model setup, we also search within our future scenario for a global ice-sheet and sea-level configuration that will bring the global hypsometric maximum (~2–5 m) to the sea surface. Specifically, we terminate our future scenario at a range of different times (i.e., different global ice-sheet configurations) and let the Earth system adjust to a steady-state sea-level configuration (until +20 kyr).

### *Global mean sea level*

In this work we investigate how changes in surface area with elevation impacts shoreline migration over time, and thus the conversion from ice-volume changes to global water-equivalent mean sea-level changes. We calculate GMSL changes relative to present day over the last glacial cycle and into the future using either a fixed ocean area ($\Delta GMSL_{fixed}$) or a time-varying ocean area ($\Delta GMSL_{hyp}$). So, although the sea-level model used here includes shoreline migration, these different GMSL calculations demonstrate the consequence of excluding time-varying shorelines and how this assumption will modulate the conversion from ice-volume changes to global water-equivalent mean sea-level changes in a manner that depends on Earth's particular hypsometry.

We adopt the approach by Rowley (2017) and calculate GMSL by summing the integral of the hypsometric curve from the deepest ocean up to the ocean surface for every timestep (Fig. 3A). Since mass conservation is inherent to our global model formulation, changes in global ocean volume correspond directly to water-equivalent ice-volume changes. This method will automatically include local effects on ocean geometry associated with the influx of water into areas freed of marine-based ice and the subsequent outflux of water as these areas begin to rebound (e.g., Pan et al., 2021; Fig. 3B), as well as other changes in global sea level that result from GIA-driven changes across the entire ocean basin. Therefore, the difference between the two $\Delta GMSL$ calculations is due only to the time-varying ocean area that the changing water volume is distributed over (Fig. 3B).

$\Delta GMSL_{hyp}$ is defined as (e.g., Milne and Mitrovica, 2008):

$$\Delta GMSL_{hyp}(t) = \int_{t=0}^{t} \frac{\Delta \dot{V}_{ocean}(t)}{A_{ocean}(t)} dt \quad (1)$$

where $\Delta \dot{V}_{ocean}$ represents the rate of change in ocean volume and $A_{ocean}(t)$ is the time-varying ocean area calculated using the hypsometry-driven land fraction that we track throughout the model. In contrast, $\Delta GMSL_{fixed}$ is given by:

$$\Delta GMSL_{fixed}(t) = \frac{\Delta V_{ocean}(t)}{A_{present\ ocean}} \quad (2)$$

where $A_{present\ ocean}$ represents present-day ocean area (71%) and $\Delta V_{ocean}$ is the total change in ocean volume (i.e., water-equivalent ice-volume change) relative to present day.

For comparison, we also consider the approach of Pan et al. (2021) in our calculations of future sea level, which excludes from the GMSL calculation any area exposed by retreating of grounded marine-based ice (henceforth $\Delta GMSL_{Pan}$). The equation governing this calculation is identical to Eq. (1) except that the surface integral does not include regions of future marine ice-sheet retreat and these regions are also excluded from the area term in the denominator. The Pan et al. (2021) definition was designed to consider the mean sea-level change in the "open" ocean during grounded ice retreat and was not intended as a strictly global measure, but computing it provides insight into the relative contribution to $\Delta GMSL_{hyp}$ from post-glacially uplifting sectors of retreat and the rest of the global ocean. We also consider a GMSL definition consistent with Adhikari et al. (2020) that was designed for regional ice modeling. This definition departs from $\Delta GMSL_{hyp}$ by not including shoreline migration outside the area of ice cover.

## Results

### *Global hypsometry and land fraction*

Different parts of the global hypsometric distribution are dominated by different regions (Fig. 1A-C). In the vicinity of the present-day sea surface (Fig. 1B), the global hypsometric curve is largely dominated by African hypsometry between ~250–1,100 m a.s.l., whereas the hypsometric maximum ~90–140 m a.s.l. stems mainly from South America and Asia. A few peaks below the present-day sea surface result mainly from North America (~18 m and 45 m below) and Asia (~26 m below). Australia also shows a significant hypsometric maximum ~55 m below the present-day sea surface. These hypsometric features are also evident as trends in the regional cumulative surface area (Fig. 1D), where they are seen as a change in slope. All regions except Antarctica show a narrow hypsometric maximum limited to the 0-m elevation bin (Fig. 1C,

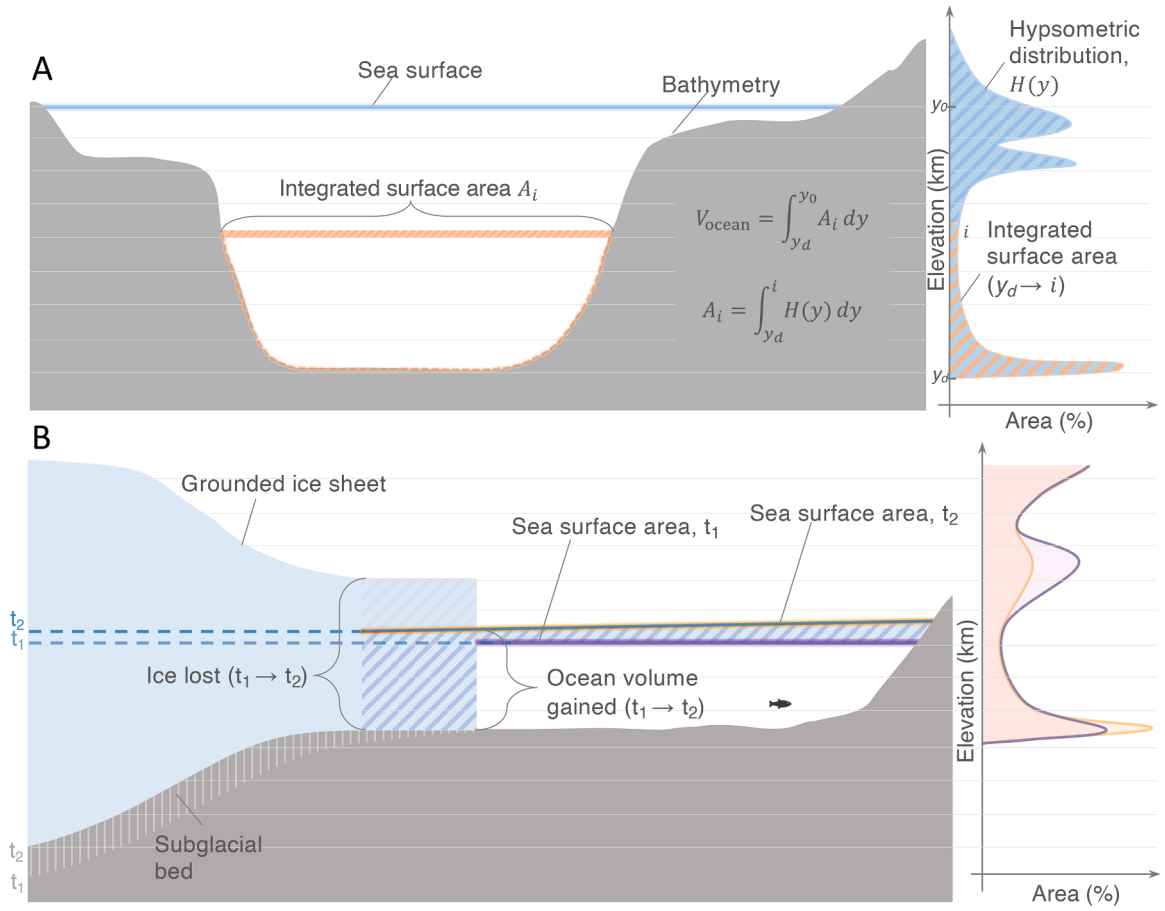


**Fig. 3.** Schematic illustration of GMSL concepts. A, definition of ocean volume ($V_{ocean}$), based on the integration of surface area ($A_i$) for each depth ($i$) in the global ocean, that is found by integration of the hypsometric curve, i.e., surface area ($H$) with elevation ($y$), from the deepest part of the ocean up to a given depth. The three peaks in the hypsometric curve arise from the ocean bottom, and the two shallow bathymetry regions, respectively. B, illustration of the difference in sea-surface area that arises because of shoreline migration and the retreat (or growth) of grounded marine-based ice sheets as well as ocean volume gained and the resulting hypsometric distributions. Note that we do not consider floating ice shelves here nor a change in crustal elevation related to added ocean water which will also provide accommodation space for meltwater.

open circles at 0 m). These regions also show an additional maximum in the vicinity of the present-day sea surface (Fig. 1C, open circles above 0 m elevation), with the exception of North America (including Greenland) and Europe that show a slightly wider maximum at 0 m instead. These additional hypsometric maxima are all located within 10 m of the present-day sea surface. The resulting global hypsometric maximum for the GEBCO Compilation Group (2023) DEM is found +5 m above the present-day sea surface.

With the exception of Antarctica, the various regions show significant changes in cumulative surface area within a few hundred meters of the present-day sea surface, and a concave upward trend in cumulative surface area towards higher elevations (Fig. 1D). Antarctic hypsometry is dominated by the presence of the AIS (wide hypsometric maximum centered at ~3 km elevation) and the downwards shifting of the surrounding continental shelf regions due to the weight of the AIS (hypsometric maximum and a break-in-slope in cumulative surface area ~450–500 m below the present sea surface; Fig. 1A, red curve).

As global sea level fell during the last glacial cycle, the +5-m global hypsometric maximum shifted upwards (Fig. 4A, 5A, Fig. S2A) reaching a highest elevation of ~113 m a.s.l. during the Last Glacial Maximum (LGM) at 26 ka in the ICE6G_C ice model. The same pattern is seen for most regions (Fig. S3), although some deviations occur due to regional changes in the shape of the hypsometric curve as well as the resulting GIA that drives geographically non-uniform shifts in topography (e.g., for North America, including Greenland; Fig. S3A). This shift in elevation of the global hypsometric maximum at the LGM constitutes only ~83% of the concurrent GMSL change from the LGM to modern (113 m versus 136 m; Fig. 5A,C). The cumulative surface area also shifts upwards from the last interglacial and into the LGM (Fig. 4B, Fig. S2B), slowly increasing the land fraction to a maximum of 34% (Fig. 5A, blue curve).

We note that the global hypsometric maximum was sitting at the sea surface in the Mid Holocene between ~6,500–6,000 yrs BP. Since the ICE6G_C model has only marginal melting in the past 6,000 yrs, the adjustment in the elevation of the hypsometric maximum since Mid Holocene is dominated by the GIA process rather than changes in ice volume. We return to this key observation below.

For our future scenario, the +5-m global hypsometric maximum shifts downwards relative to the rising sea level, reaching a minimum elevation of ~59 m below the sea surface, before it slowly moves upwards and converges at ~55 m below the sea surface ~15 kyr into the future (Fig. 4A, Fig. S2C, Fig. 5A). This final reversal in the elevation of the hypsometric maximum of a few meters takes place ~8,000 yrs into the future when the AIS (for our extreme scenario) is limited to small glaciers and ice caps in the Transantarctic mountains (Fig. 5B). Any subsequent changes in hypsometry and regional sea level are driven mainly by residual GIA.

Most regions show a similar downward shift of ~55 m in the future elevation of their hypsometric maximum (Fig. S3), although for North America including Greenland the shift is >100 m, owing to the nature of the hypsometric curve near sea level (Fig. S3A). We note that the global elevation shift constitutes only ~77% of the concurrent GMSL change

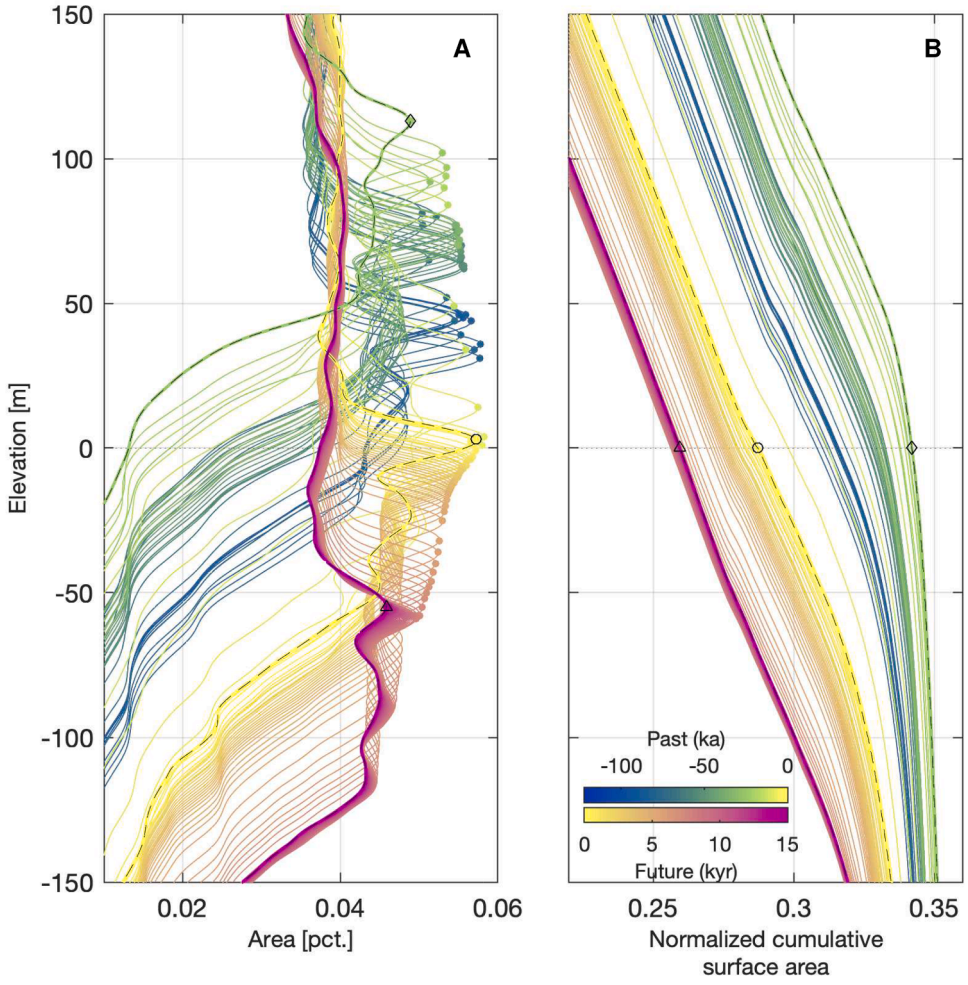


**Fig. 4.** Transient hypsometry and cumulative surface area. A, global hypsometric distribution for each time step in our global sea-level model simulation after a burn-in phase of 30 kyr, from 92 ka until 15 kyr into the future (age indicated by color according to legend in B), for the elevation interval between −150 m and +150 m. We note that the hypsometric curves are smoothed, leading to a merging of the 0-m and the 5-m hypsometric maxima (e.g., gray curve in Fig. 1C). The global (near-sea-level) hypsometric maxima are marked for each time step with a solid circle, while hypsometric maxima for the LGM, the present day, and the end of the simulation are highlighted by an open diamond, circle, and triangle, respectively. The hypsometric curves for the LGM, present day, and end of the simulation are highlighted by black dashed lines. B, Normalized cumulative surface area for each time step in our global sea-level simulation after a burn-in phase of 30 kyr, from 92 ka until 15 kyr into the future. The land fraction at sea level is highlighted for the LGM, present day, and the end of the model with an open diamond, circle, and triangle, respectively. We note than an alternative version of this figure is available as Fig. S2, showing past and future curves in separate panels.

(Fig. 5A,C), emphasizing again that there is not a one-to-one relationship between a given sea-level change and the resulting change in elevation of the hypsometric maximum. During our future scenario, the land fraction drops below 26% as the cumulative surface-area curve shifts downwards relative to the rising sea level (Fig. 4B, Fig. S2D).

*Global hypsometry and global mean sea level*

When calculating GMSL changes using a fixed (present-day) ocean area, we predict a GMSL fall of ~130.3 m relative to present day for the LGM ($\Delta GMSL_{fixed}$; Fig. 5C). In contrast, the analogous value for $\Delta GMSL_{hyp}$ is ~136.3 m (Fig. 5C). The larger magnitude is explained by a reduced ocean area as sea level is lowered, requiring a larger sea-level fall for $\Delta GMSL_{hyp}$ to accommodate the same change in ocean volume. For our future scenario, $\Delta GMSL_{fixed}$ reaches a maximum of ~72.9 m when both the GrIS and AIS have melted away completely and GIA has equilibrated to the new state (Fig. 5C), whereas $\Delta GMSL_{hyp}$ reaches a maximum of ~71.1 m. The difference arises because the hypsometry-driven decrease in land fraction will require a smaller sea-level rise to accommodate the same change in ocean volume compared to a situation with a fixed ocean basin. The difference between $\Delta GMSL_{fixed}$ and $\Delta GMSL_{hyp}$ is explored in more detail in Fig. S4.

The distinct slopes in the cumulative surface area for different regions (Fig. S3) influence their relative changes in land fraction (flooded area) over time (Bond, 1978). This influence of Earth's hypsometry and global variations in cumulative surface area on flooding is visualized in a global flooding-age map (Fig. 6A). Specifically, we extract the time where each cell in the grid evolves from being part of the land mask to being part of the ocean mask. Here, we focus on the large changes in land fraction from the LGM onwards and map the last time a region was flooded since ~21 ka. Regions with low (<15 m/percent) negative slopes in their cumulative surface area near the present-day sea surface (Fig. 1C; Europe, North America, and Asia) show the largest changes in flooding area over the last glacial cycle (16.8%, 9.4%, and 7.8%, respectively; Fig. 6B), as well as among the largest fractional changes during future flooding (−5.4%, −2.9%, and −4.9%, respectively). Conversely, the regions that show relatively steep (>20 m/pct.) negative slopes (Fig. 1C; South America, Africa, and Australia) saw smaller land-fraction changes during the past glaciation (1.9%, 2.6%, and 5.4%, respectively; Fig. 6B), while the future scenario predicts smaller land-fraction changes (−1.4%, −2.4%, and −2.2%, respectively).

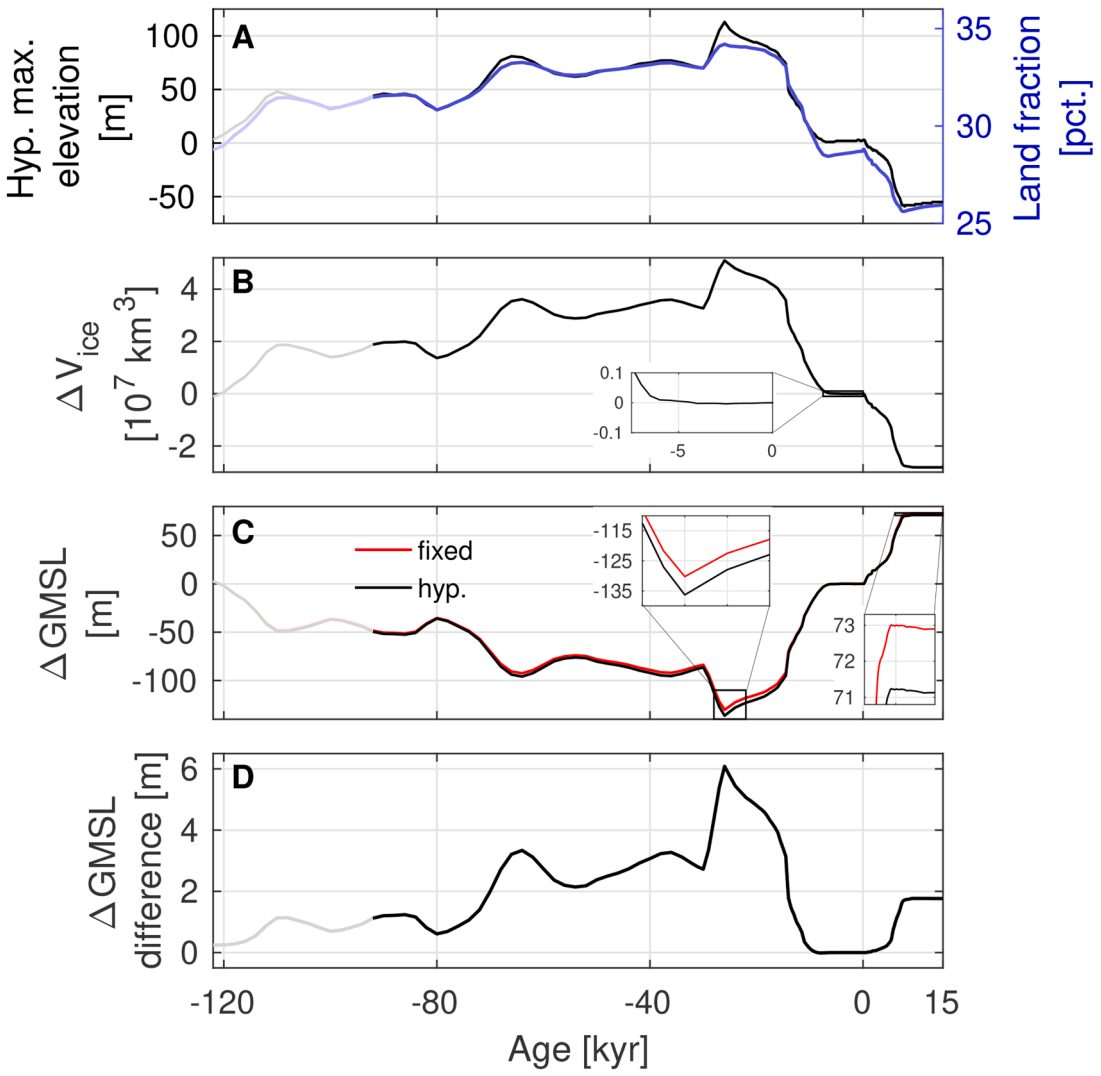


**Fig. 5.** Evolution in global mean sea level (GMSL) relative to present. A, Evolution in the global (near-sea-level) hypsometric maximum (smoothed; black curve) and the land fraction at sea level (blue curve). B, Evolution in grounded ice volume. C, Evolution in GMSL relative to present, calculated using two different approaches (fixed versus hypsometric (hyp.); see text for explanation). C, Difference between the GMSL approaches 'fixed' and 'hyp.'. A burn-in phase of 30 kyr is indicated on all panels with transparent colors.

*An alternate GIA model*

We repeated our calculations over the last glacial cycle using an alternative GIA model (PaleoMIST; Gowan et al. 2021). This ice-sheet reconstruction has a temporal resolution of 2,500 yrs over the last 80 ka and is coupled to a 1D viscoelastic Earth model characterized by a lithospheric thickness of 120 km, and upper and lower mantle viscosities of $4 \times 10^{20}$ Pa s and $4 \times 10^{22}$ Pa s, respectively. Using this model, we predict a minor dip of ~1 m in elevation of the hypsometric maximum to a minimum of +4 m at 2,500 yrs BP before moving to +5 m at present. This muted signal over the current interglacial, compared to the ICE6G_C/VM5a simulation that places the hypsometric maximum at the sea surface at 6,500 yrs BP, is due to both ongoing melt in the PaeloMIST model (Fig. S5B), which compensates for the GIA-induced rise in the hypsometric maximum over the period, and higher mantle viscosity of the Earth model relative to VM5a, which slows the GIA response.

The PaleoMIST model predicts a larger shift in the hypsometric maximum over a glacial cycle, up to +120 m at the LGM, while the associated sea-level fall is less pronounced for both $\Delta GMSL_{fixed}$ (123.9 m) and $\Delta GMSL_{hyp}$ (130.3 m) relative to our standard model simulation (Fig. S5). The difference between $\Delta GMSL_{fixed}$ and $\Delta GMSL_{hyp}$ of ~6.4 m is moderately larger than the analogous result based on ICE6G_C/VM5 (~6.0 m).

*Hypsometry projections*

We searched within our future scenario for a global ice-sheet and steady-state sea-level configuration that will bring the +5-m hypsometric maximum of GEBCO Compilation Group (2023) in accordance with the sea surface. That is, we halted ice-sheet melting at different times in the future portion of our simulation and allowed the model to reach steady state. Following this exercise, we find that a cessation of melting 986 yrs into the future yields a GMSL rise of 8.6 m and ultimately brings the +5-m hypsometric maximum down to the sea surface (GMSL refers to $\Delta GMSL_{hyp}$ here and onwards unless specified otherwise; Fig. 7). At this time in our future scenario, the entire GrIS and parts of AIS have melted away (Fig. 7B). Allowing the Earth system to adjust to steady-state for this ice-sheet configuration results first in a significant sea-level rise due largely to ice-mass changes that initially brings the +5-m hypsometric maximum down to −3 m (Fig. 7C). However, continuing GIA effects associated with the full ice-sheet history of our simulation eventually raise the hypsometric maximum to ~0 m (Fig. 7C), albeit with large regional variations in relative sea-level change (Fig. 7A).

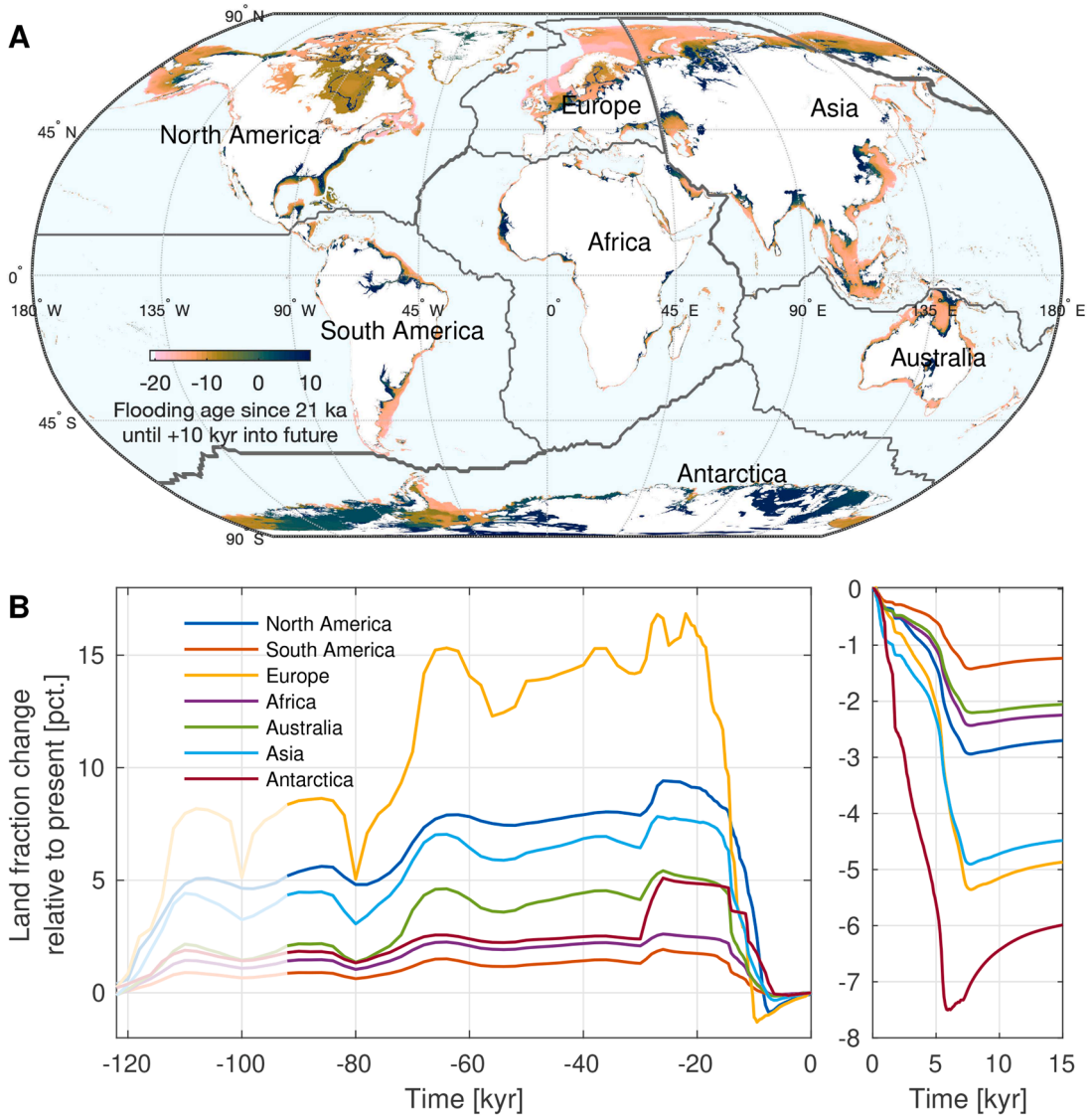


**Fig. 6.** Global flooding map and regional land-fraction changes. A, map showing the timing of flooding since the last deglaciation (since ~21 ka). We note that regions may not stay submerged owing to GIA effects that outpace GMSL changes. B, Changes in land fraction relative to the present day for each region, for the last glacial cycle (left panel) and the future scenario (right panel), respectively. A spin-up phase of 30 kyr is indicated with transparent colors.

For comparison, we also considered the case where no future ice melt is introduced, to discern the GIA effect associated solely with the last glacial cycle. We found that the present-day hypsometric maximum at +5 m rises 2 m, ultimately converging at +7 m above the sea surface (Fig. S6A). This indicates that the rise of the hypsometric maximum from −3 m to ~0 m that we observe in our future +8.6 m GMSL state is dominated by the Earth's response to past ice-mass changes.

Other definitions of GMSL following the retreat of grounded, marine-based ice have been suggested for a range of different applications (e.g., Adhikari et al., 2020; Goelzer et al., 2020; Pan et al., 2021). Using the Pan et al. (2021) definition, which does not include regions exposed by retreating marine-based ice in the calculation of GMSL ($\Delta GMSL_{Pan}$), we can isolate the impact of uplifted marine-based ice sectors on GMSL. For the same ice-loss scenario, we find that $\Delta GMSL_{Pan}$ is smaller (+7.7 m) compared to $\Delta GMSL_{hyp}$ (+8.6 m) because the uplift of previously glaciated marine sectors leads to a loss of ocean volume in these sectors and an equal gain in ocean volume beyond these sectors.

GMSL change, as defined in the approach of Adhikari et al. (2020), was designed for regional ice-sheet modelling results. Their definition is similar to $\Delta GMSL_{hyp}$ in that it adopts the margin of grounded, marine-based ice as the perimeter of the ocean, but it does not – since it is a regional study – include coastline migration in the open ocean. The impact of ignoring this latter effect on the computed GMSL change due to future melting is significantly smaller than the impact of adopting $\Delta GMSL_{Pan}$, deviating only by 0.02 m from the +8.6 m rise associated with $\Delta GMSL_{hyp}$.

## Discussion

### *Global hypsometry and global mean sea level*

While GMSL change has in principle limited practical meaning since few places will experience this precise sea-level change, the concept is commonly used in the sea-level literature and is of particular importance at the intersection between paleo and modern ice-sheet and sea-level research. GMSL change is also widely used to quantify future projections of ice-sheet contributions. However, the exact approach used to calculate GMSL changes is often not detailed explicitly and different approaches exist (e.g., Simms et al., 2019; Dumitru, et al., 2019; Gregory et al., 2019; Adhikari et al., 2020; Goelzer et al., 2020; Pan et al., 2021).

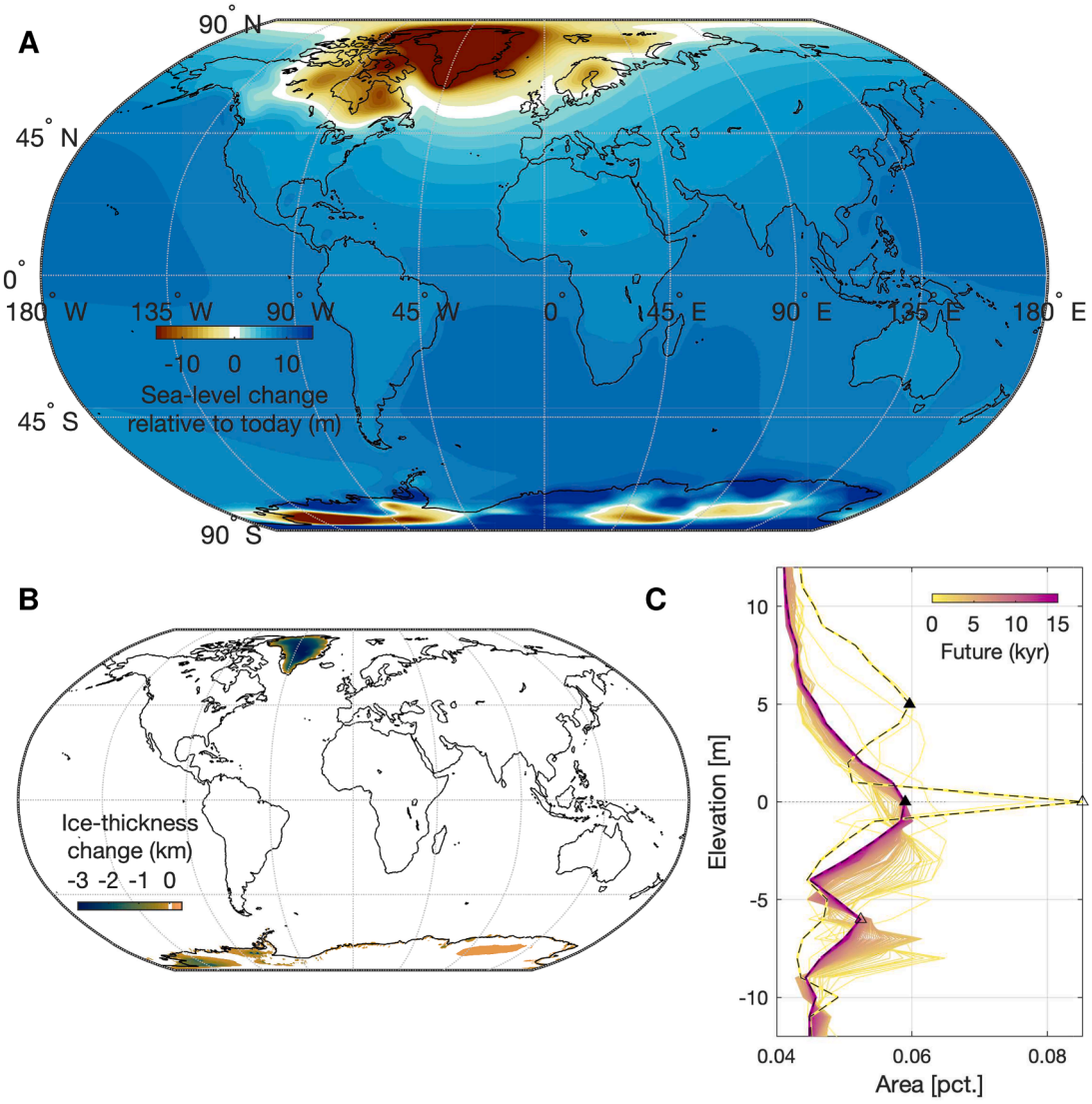


**Fig. 7.** A, Sea-level change relative to today for the steady state +8.6 m sea-level world. We note that the colormap is saturated for regions that have experienced large changes in ice thickness (Greenland and Antarctica, see B), to emphasize GMSL changes. B, Ice-thickness changes for this state relative to present day. C, Evolution in the sea-surface-near hypsometric distribution (and hypsometric maxima) for this state of global ice-configuration and sea level, showing the future evolution only. Triangles highlight the elevation of hypsometric maxima today and in the future steady-state +8.6 m sea level world, where the present-day 5-m hypsometric maximum has been shifted to 0 m.

The effect of hypsometry on GMSL change is significant, particularly for past sea-level low stands such as the LGM, where the inclusion of Earth's hypsometry (i.e., allowing shorelines to migrate as sea levels change) makes a difference of ~6 m for the GMSL calculation ($\Delta GMSL_{hyp}$ versus $\Delta GMSL_{fixed}$), whereas the effect is more modest for our extreme near-ice-free future scenario (~2 m; Fig. 5D).

In our future scenario we found that a steady-state GMSL change of +8.6 m associated with ~33 × $10^5$ $km^3$ of ice melt over nearly 1,000 yrs brought the present-day +5-m hypsometry maximum down to 0 m. To test the robustness of this result, we repeated the calculation using an alternative ice-melt scenario with a significantly different time scale for AIS demise (~5 kyr versus ~10 kyr; Fig. S7). This alternative ice-melt scenario requires a moderately larger GMSL change of +9.0 m continuing until 725 yrs into the future to bring the hypsometric maximum to the sea surface. The impact on the non-linearity associated with the effect of hypsometry on GMSL (Fig. S4) is negligible (Fig. S8C).

*Earth's hypsometry and "normal" state*

Our DEM analysis demonstrates that the hypsometric distributions of most regions show a maximum just above the present-day sea surface in addition to a narrow peak at 0 m (Fig. 1C). These additional maxima range from ~1–6 m elevation compared to the global average maximum at +5 m in GEBCO Compilation Group (2023). Antarctica does not show any hypsometric maxima near the present-day sea surface, whereas we speculate that the wider maxima at 0 m for North America and Europe may arise because the expected narrow 0-m maximum is indistinguishable from an additional hypsometric maximum near 0 m (present in earlier data products; GEBCO Compilation Group, 2021). The global +5-m maximum is prevalent across several elevation bins and has been a robust feature between GEBCO data releases, whereas the 0-m hypsometric maximum is represented by a single elevation bin and could be a technical artefact introduced since 2022, with at least 40% of the 0-m values in GEBCO Compilation Group (2023) resulting from interpolation (Fig. 2; Global GEBCO Center, personal communication).

As noted earlier, several recent 'corrected' digital surface models (e.

g., Pronk et al., 2024) find the hypsometric maximum somewhat lower than is recorded in the global GEBCO data sets, specifically ~2–4 m above the present sea surface instead of +5 m. These data products correct DEMs using lidar data or regression methods to remove non-terrain cells (e.g., vegetation or human infrastructure) and fill these gaps with interpolation. While these new data products ostensibly produce a more accurate result, they are not available globally, or are at a high spatial resolution, making then unsuited for global applications. Nevertheless, in the following discussion, this uncertainty must be kept in mind.

The distinct shape of Earth's hypsometry near the present-day sea surface is a competition between long-term solid-Earth processes (e.g., dynamic topography, tectonics, GIA) that deform the Earth from within and climate-dependent processes that erode and redistribute material at the surface of the Earth. However, the time scales of these processes and their interactions are not fully understood (e.g., Molnar and England, 1990; Burbank et al., 1996; Willett, 1999; Reiners et al., 2003; von Blanckenburg, 2006; Koppes and Montgomery, 2009; Whipple, 2009). Rowley (2013) proposed that the distinct hypsometric maximum at the present-day sea surface could suggest either 1) the time needed for Earth's hypsometry to adjust to a changing sea level is short relative to the above processes, or 2) long-term ($10^7$–$10^8$ yr) mean sea level has not varied significantly from its present height, or both. The present-day global hypsometric maximum we have identified above the sea surface, at +5 m for the GEBCO Compilation Group (2023) DEM, adds insight and nuance to these arguments that we explore below by considering processes that may contribute to this feature.

We hypothesize that GIA is responsible for the present-day elevation of the global hypsometric maximum. This hypothesis is supported by our calculation demonstrating that a GIA simulation based on the ICE6G_C/VM5a model shifted the global maximum from 0 m to +5 m over the past ~6,000 yrs (Fig. 8). 6,000 yrs BP marks a time of transition in the ocean from a period of melt-dominated sea-level rise with progressive and rapid lowering of the hypsometry curve to a period of negligible sea-level change but non-negligible rising of the hypsometric maximum. This latter rise in the hypsometric maximum stems from a net uplift of continents and subsidence of ocean basins from the LGM onward because of mass transfer from land to the ocean. Given the ~1:2 ratio of continental versus oceanic areas, the net uplift rate on continents will be twice the rate of ocean basin subsidence. This process is continuously active, albeit at higher rates during most of the post-LGM phase, but prior to the last ~6,000 yrs it is swamped by the volume of meltwater entering the ocean. The adjustment of the hypsometric maximum since 6,000 ka BP is also influenced by spatially variable sea-level changes that change the shape of the hypsometric curve, largely related to the processes of continental levering and ocean syphoning (e.g., Mitrovica

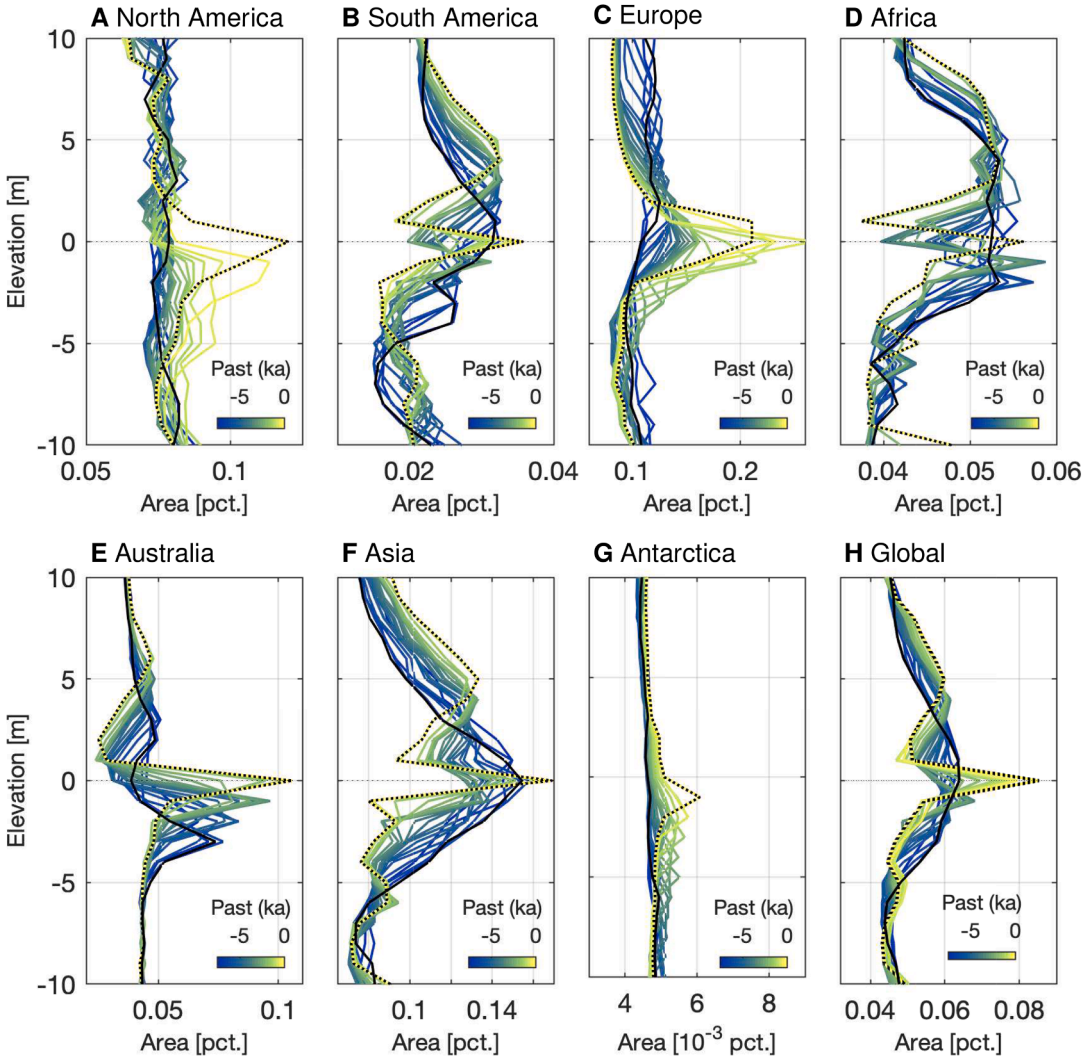


**Fig. 8.** Hypsometry from 7,500 yrs BP until present day for distinct regions: A, North America; B, South America; C, Europe; D, Africa; E, Australia; F, Asia; G, Antarctica. H, The equivalent global hypsometry. The present-day curves are highlighted with a dotted black line while the curves representing 6,500 yrs BP (timing of minimum elevation of the global hypsometric maximum in the Holocene) are highlighted in black.

and Milne, 2002).

If GIA is an explanation for Earth's hypsometric maximum ~2–5 m above the sea surface, it implies that geomorphic processes of erosion and sedimentation were rapid enough to establish a global scale record of mean shoreline position at the end of the last deglaciation phase but not rapid enough to erode all evidence of this record in the subsequent ~6,000 yrs. One test of this hypothesis, though potentially complicated by regional variations in lithology, is to compare the magnitude of the predicted changes in hypsometry due to GIA within different regions, with the variability in the elevation of the hypsometric maxima shown in Fig. 1C. To this end, we find that for three regions – Asia, South America, and Africa – the hypsometric maxima observed today at ~5 m, ~4 m, and ~3–7 m, respectively, are all predicted to be at a consistent elevation at the sea surface at ~6,500 yrs BP (Fig. 8B, D, F). The hypsometric maxima of the other regions either show inconclusive patterns since ~6,500 yrs BP (Antarctica, North America, and Europe; Fig. 8A, C, G), or show a shift that does not correspond to the present elevation of the hypsometric maximum (Australia; Fig. 8E). We conclude that GIA is the primary driver of the present-day hypsometric maximum, although it is also possible that other processes must play a role since not all regional hypsometric maxima are reconstructed to a consistent elevation ~6,500 yrs BP.

As we noted above, barring future melting, the ongoing GIA process will ultimately raise the present-day hypsometric maximum by an additional 2 m, to +7 m for GEBCO Compilation Group (2023), or to +4–7 m if we consider the uncertainty in the present-day elevation. This raises an interesting question, namely, what longer term processes may also have contributed non-negligibly to a "GIA-converged maximum" at this level?

One possibility is that the GIA-converged maximum reflects in part a more normal level of the sea surface (and ice volume) during Pleistocene interglacials that remains imprinted in the geological record of topography. A complexity for this suggestion is that in addition to GIA-driven changes in hypsometry, previous interglacials such as MIS 5e (Kopp et al., 2009; Dutton and Lambeck, 2012) and MIS 11 (Raymo and Mitrovica, 2012) were characterized by ice volumes significantly smaller (and GMSL higher) than at present day. In this case, the GIA-converged maximum may represent some spatial (across the globe) and temporal (i.e., across multiple interglacials) average of the level of the sea surface over the timescale of several glacial cycles ($10^5$–$10^6$ yrs). However, we note that the timing as well as the amplitude of the high stand depends strongly on the timing and amplitude of the excess ice melt (Dutton and Lambeck, 2012; Raymo and Mitrovica, 2012). The regional variability in the GIA-converged hypsometry may provide a test of this hypothesis.

A second possibility is that the GIA-converged maximum represents, in part, the mean level of the sea surface over a much longer, multi-million-year time window. This would be a variation of the argument by Rowley (2013) in the sense that it is not the present-day sea surface that represents the normal mean level of the sea surface, and ice volume, but rather some fraction of the GIA-converged maximum reflects Earth's normal mean sea level. An example that may be of relevance would be hypsometry and ice volume in the time period after inception and stabilization of the Antarctic Ice Sheet and prior to the onset of northern hemisphere glaciation (Zachos et al., 2001).

As we have noted, the two possibilities discussed above imply a normal state with less global ice volume than at present day. These conjectures are consistent with the consensus that mean temperatures and global sea level were higher than at present during several previous interglacials (e.g., Rohling et al., 2009; Dutton et al., 2015) and, more generally, over the Plio-Pleistocene and beyond (e.g., Zachos et al., 2001; Tierney et al., 2020).

A third possibility is that the GIA-converged maximum has a contribition from long-term trends in erosion and deposition. The models presented here do not include erosion and deposition, or the associated effects these processes may have on hypsometry, GIA, and sea level (e.g., Whitehouse, 2018). While erosion and deposition have proven important for sea-level change on a regional scale, even on time scales of a single glacial cycle (e.g., Ruetenik et al., 2020; Jungdal-Olesen et al., 2023), their potential influence on sea level on a global scale is yet to be quantified. In addition, glacially dominated surface processes, such as the carving of deep fjords below sea level has been shown to elevate regional topography significantly in previously glaciated regions (e.g., Kessler et al., 2008; Pedersen et al., 2021), but herein we do not see such patterns in the present-day hypsometric distributions of previously glaciated regions (e.g., for North America and Europe).

Finally, if long-term preservation is possible, dynamic topography (e.g., Mitrovica et al., 1989; Gurnis, 1990a, b; Moucha et al. 2008, Petersen et al., 2010; Conrad, 2013; Flament et al., 2013) may also play a role in the present-day hypsometric maximum, and the process, together with more localized tectonic effects, would impart a regional signal on the present-day hypsometry and the GIA-converged maximum.

We emphasize once again that our model simulations demonstrate that a one-to-one relation does not exist between GMSL changes and the resulting elevation of the global hypsometric maximum. Indeed, as we have noted, the computed shift in the hypsometric maximum from 0 m to +5 m over the past ~6,000 yrs occurs during a period where GMSL changes by <1 m, whether defined as we have by $\Delta GMSL_{hyp}$or with $\Delta GMSL_{fixed}$. Moreover, a future GMSL rise of ~9 m discussed in our simulations only shifts the current +5-m hypsometric maximum down to the sea surface, i.e., 0 m. This level of future GMSL rise would represent an upper bound if the present-day hypsometric maximum lies in the range +2–5 m.

## Conclusions

Here we have analysed Earth's hypsometry – globally and for individual regions – across a glacial cycle and into a deep future scenario. We have used a sea-level model that accurately accounts for shoreline migration due to the advance and retreat of grounded, marine-based ice and also at distance from these areas. We have focused on the distinct global hypsometric maximum above the present-day sea surface and how it has varied over the last glacial cycle and may vary as the Earth system evolves in a progressively warming world. Our analysis has emphasized the distinction between changes in sea level and hypsometry across this entire range. We find, for example, that the distinct global hypsometric maximum shifted ~113 m higher than today during the LGM whilst the GMSL change over the same period was ~136 m. Adopting a definition of GMSL change that assumes a fixed-to-present-day ocean area yields a GMSL change ~6 m smaller.

Different regions contribute differently to the global impact of Earth's hypsometry on GMSL. Indeed, regions with low-sloping trends in the cumulative surface area (Europe, North America, and Asia), show the largest changes in flooding area over the last glacial cycle and into the future, whereas the regions with relatively steep-sloping trends in the cumulative surface area (South America, Africa, and Australia) show much smaller land-fraction changes during the past glaciation and into the future. Nevertheless, we find that most regions show a hypsometric maximum just above the present-day sea surface, albeit of varying elevation.

Our results, and particularly our regional analysis of evolving hypsometry, demonstrate that GIA is the primary contributor to the present-day hypsometric maximum above the sea surface. This is supported by our GIA modelling that brings several of the regional hypsometric maxima to a consistent elevation at 0 m at the end of the last deglaciation phase (6,500 yrs BP). In this case, the present-day global hypsometric maximum has been preserved in the geological record over this time period. Ongoing GIA will ultimately raise the maximum a further 2 m, to an elevation of 4–7 m if we consider the uncertainty suggested by various DEMs. If a portion of the hypsometric maximum has persisted for longer than Holocene time scales, the GIA-converged

level implies that the longer-term mean sea-level state of the Earth may differ from today. We have speculated on three possible reasons for this longer-term mean state, including lower ice volumes during either Pleistocene interglacial high stands or prior to Pliocene onset of glaciation in the northern hemisphere, as well as global trends in erosion. Exploring these issues will deepen our understanding of this feature of the Earth's present-day topography as well the interplay between sea-level changes, variations in hypsometry, and the time scales of geomorphological processes, and this effort remains an avenue for future work.

## CRediT authorship contribution statement

**V.K. Pedersen:** Writing – review & editing, Writing – original draft, Visualization, Methodology, Formal analysis, Conceptualization. **N. Gomez:** Writing – review & editing, Methodology, Conceptualization. **J. X. Mitrovica:** Writing – review & editing, Software, Methodology, Conceptualization. **G. Jungdal-Olesen:** Writing – review & editing, Software, Methodology. **J.L. Andersen:** Writing – review & editing, Methodology. **J. Garbe:** Writing – review & editing, Resources. **A. Aschwanden:** Writing – review & editing, Resources. **R. Winkelmann:** Writing – review & editing, Resources.

## Declaration of competing interest

The authors declare that they have no known competing financial interests or personal relationships that could have appeared to influence the work reported in this paper.

## Acknowledgements

This work was supported by a research grant (15467) from VILLUM FONDEN. We thank both an anonymous reviewer and Bob Anderson for constructive comments that improved this manuscript.

## Supplementary materials

Supplementary material associated with this article can be found, in the online version, at doi:10.1016/j.epsl.2024.119071.

## Data availability

Data will be made available on request.

## References

Adhikari, S., Ivins, E.R., Larour, E., Caron, L., Seroussi, H., 2020. A kinematic formalism for tracking ice–ocean mass exchange on the Earth's surface and estimating sea-level change. Cryosphere 14, 2819–2833. https://doi.org/10.5194/tc-14-2819-2020.

Algeo, T.J., Wilkinson, B.H., 1991. Modern and ancient continental hypsometries. J. Geol. Soc. London 148, 643–653.

Argus, D.F., Gordon, R.G., DeMets, C., 2011. Geologically current motion of 56 plates relative to the no-net-rotation reference frame. Geochem. Geophys. Geosyst. 12, Q11001. https://doi.org/10.1029/2011GC003751.

Argus, D.F., Peltier, W.R., Drummond, R., Moore, A.W., 2014. The Antarctica component of postglacial rebound model ICE-6G_C (VM5a) based on GPS positioning, exposure age dating of ice thicknesses, and relative sea level histories. Geophys. J. Int. 198, 537–563. https://doi.org/10.1093/Gji/Ggu140.

Aschwanden, A., Fahnestock, M.A., Truffer, M., Brinkerhoff, D.J., Hock, R., Khroulev, C., Mottram, R., Khan, S.A., 2019. Contribution of the Greenland Ice Sheet to sea level over the next millennium. Sci. Adv. 5, eaav9396. https://doi.org/10.1126/sciadv.aav9396.

Becker, J.J., Sandwell, D.T., Smith, W.H.F., Braud, J., Binder, B., Depner, J., Fabre, D., Factor, J., Ingalls, S., Kim, S.H., Ladner, R., Marks, K., Nelson, S., Pharaoh, A., Trimmer, R., von Rosenberg, J., Wallace, G., Weatherall, P., 2009. Global bathymetry and elevation data at 30 ′onds resolution: srtm30_plus. Mar Geod 32, 355–371. doi:10.1080/01490410903297766.

Bird, P., 2003. An updated digital model of plate boundaries. Geochem. Geophys. Geosyst. 4 (3), 1027. https://doi.org/10.1029/2001GC000252.

Bond, G., 1978. Evidence for Late Tertiary uplift of Africa relative to North America, South America, Australia and Europe. J. Geol. 86, 47–65.

Brozovic, N., Burbank, D.W., Meigs, A.J., 1997. Climatic limits on landscape development in the Northwestern Himalaya. Science (1979) 276, 571–574.

Burbank, D.W., Leland, J., Fielding, E., Anderson, R.S., Brozovic, N., Reid, M.R., Duncan, C., 1996. Bedrock incision, rock uplift and threshold hillslopes in the northwestern Himalaya. Nature 379, 505–510.

Conrad, C.P., 2013. The solid Earth's influence on sea level. GSA Bulletin 125 (7/8), 1027–1052. https://doi.org/10.1130/B30764.1.

Dumitru, O.-A., Austermann, J., Polyak, V.J., Fornós, J.J., Asmerom, Y., Ginés, J., Ginés, A., Onac, B.P., 2019. Constraints on global mean sea level during Pliocene warmth. Nature 547, 233–236. https://doi.org/10.1038/s41586-019-1543-2.

Dutton, A., Carlson, A.E., Long, A.J., Milne, G.A., Clark, P.U., DeConto, R., Horton, B.P., Rahmstorf, S., Raymo, M.E., 2015. Sea-level rise due to polar ice-sheet mass loss during past warm periods. Science 349 (6244), aaa4019. https://doi.org/10.1126/science.aaa4019.

Dutton, A., Lambeck, K., 2012. Ice volume and sea level during the last interglacial. Science (1979) 337, 216–219.

Egholm, D.L., Nielsen, S.B., Pedersen, V.K., Lesemann, J.-E., 2009. Glacial effects limiting mountain height. Nature 460 (7257), 884–887.

Farrell, W.E., Clark, J.A., 1976. On postglacial sea level. Geophys. J. Roy. Astr. S. 46, 647–667.

Garbe, J., Albrecht, T., Levermann, A., et al., 2020. The hysteresis of the Antarctic Ice Sheet. Nature 585, 538–544. https://doi.org/10.1038/s41586-020-2727-5.

GEBCO Compilation Group (2021) GEBCO_2021 Grid 10.5285/c6612cbe-50b3-0cff-e053-6c86abc09f8f.

GEBCO Compilation Group (2022) GEBCO_2022 Grid doi:10.5285/e0f0bb80-ab44-2739-e053-6c86abc0289c.

GEBCO Compilation Group (2023) GEBCO_2023 Grid doi:10.5285/f98b053b-0cbc-6c23-e053-6c86abc0af7b.

Goelzer, H., Coulon, V., Pattyn, F., de Boer, B., van de Wal, R., 2020. Brief communication: on calculating the sea-level contribution in marine ice-sheet models. Cryosphere 14, 833–840. https://doi.org/10.5194/tc-14-833-2020.

Gomez, N., Mitrovica, J.X., Huybers, P., Clark, P.U., 2010. Sea level as a stabilizing factor for marine-ice-sheet grounding lines. Nat. Geosci. 3, 850–853.

Gomez, N., Yosefi, M., Pollard, D., Deconto, R.M., Sadai, S., et al., 2024. The influence of realistic 3D mantle viscosity on Antarctica's contribution to future global sea levels. Sci. Adv. 10, eadn1470. https://doi.org/10.1126/sciadv.adn1470.

Gregory, J.M., Griffies, S.M., Hughes, C.W., Lowe, J.A., Church, J.A., Fukimori, I., Gomez, N., Kopp, R.E., Landerer, F., Le Cozannet, G., Ponte, R.M., Stammer, D., Tamisiea, M.E., Van de Wal, R.S., 2019. Concepts and terminology for sea level: mean, variability and change, both local and global. Surv. Geophys. 40 (6), 1251–1289.

Gurnis, M., 1990a. Plate-mantle coupling and continental flooding. Geophys. Res. Lett. 17 (5), 623–626. https://doi.org/10.1029/GL017i005p00623.

Gurnis, M., 1990b. Ridge spreading, subduction, and sealevel fluctuations. Science (1979) 250 (4983), 970–972. https://doi.org/10.1126/science.250.4983.970.

Hell, B., Jakobsson, M., 2011. Gridding heterogeneous bathymetric data sets with stacked continuous curvature splines in tension. Mar. Geophys. Res. 32 (4), 493–501. https://doi.org/10.1007/s11001-011-9141-1.

Flament, N., Gurnis, M., Müller, R.D., 2013. A review of observations and models of dynamic topography. Lithosphere 5, 189–210. https://doi.org/10.1130/L245.1.

Harrison, C.G.A., Miskell, K.J., Brass, G.W., Saltzman, E.S., Sloan, J.L., 1983. Continental hypsography. Tectonics. 2, 357–377.

Inmann, J., 1835. Navigation and Nautical Astronomy: for the use of British Seamen, third ed. C. & J. Rivington, London, UK. https://books.google.dk/books?id=-fUOnQEACAAJ.

Kessler, M.A., Anderson, R.S., Briner, J.P., 2008. Fjord insertion into continental margins driven by topographic steering of ice. Nat. Geosci. 1, 365–369. https://doi.org/10.1038/ngeo201.

Kopp, R.E., Simons, F.J., Mitrovica, J.X., Maloof, A.C., Oppenheimer, M., 2009. Global and local sea levels during the Last Interglacial: a probabilistic assessment. Nature 462, 863–867, 2009.

Jungdal-Olesen, G., Pedersen, V.K., Andersen, J.L., Gomez, N., Mitrovica, J.X., 2023. Sea level response to late Pliocene-Quaternary erosion and deposition in Scandinavia. Quat. Sci. Rev. 301, 107938. https://doi.org/10.1016/j.quascirev.2022.107938.

Kendall, R.A., Mitrovica, J.X., Milne, G.A., 2005. On post-glacial sea level – II. Numerical formulation and comparative results on spherically symmetric models. Geophys. J. Int. 161, 679–706. https://doi.org/10.1111/j.1365-246X.2005.02553.x.

Koppes, M.N., Montgomery, D.R., 2009. The relative efficacy of fluvial and glacial erosion over modern to orogenic timescales. Nat. Geosci. 2, 644–647.

Milne, G.A., Mitrovica, J.X., 1996. Postglacial sea-level change on a rotating Earth: first results from a gravitationally self-consistent sea-level equation. Geophys. J. Int. 126 (3), F13–F20. https://doi.org/10.1111/j.1365-246X.1996.tb04691.x.

Milne, G.A., Mitrovica, J.X., 2008. Searching for eustasy in deglacial sea-level histories. Quat. Sci. Rev. 27, 2292–2302. https://doi.org/10.1016/j.quascirev.2008.08.018.

Mitchell, S.G., Montgomery, D.R., 2006. Influence of a glacial buzzsaw on the height and morphology of the Cascade Range in central Washington State. USA. Quat. Res. 65, 96–107.

Mitrovica, J.X., Beaumont, C., Jarvis, G.T., 1989. Tilting of continental interiors by the dynamic effects of subduction. Tectonics 8 (5), 1079–1094. https://doi.org/10.1029/TC008i005p01079.

Mitrovica, J.X., Milne, G.A., 2002. On the origin of late Holocene sea-level highstands within equatorial ocean basins. Quaternary Sci. Rev. 21, 2179–2190.

Mitrovica, J.X., Milne, G.A., 2003. On post-glacial sea level: I. General theory. Geophys. J. Int. 154, 253–267.

Molnar, P., England, P., 1990. Late Cenozoic uplift of mountain ranges and global climate change: chicken or egg? Nature 346, 29–34.

Morlighem, M., Rignot, E., Binder, T., Blankenship, D.D., Drews, R., Eagles, E., et al., 2020. Deep glacial troughs and stabilizing ridges unveiled beneath the margins of the Antarctic ice sheet. Nat. Geosci. 13, 132–137. https://doi.org/10.1038/s41561-019-0510-8.

Moucha, R., Forte, A.M., Mitrovica, J.X., Rowley, D.B., Quere, S., Simons, N.A., Grand, S. P., 2008. Dynamic topography and long-term sea-level variations: there is no such thing as a stable continental platform. Earth Planet. Sci. Lett. 271, 101–108. https://doi.org/10.1016/j.epsl.2008.03.056.

Pan, L., Powell, E.M., Latychev, K., Mitrovica, J.X., Creveling, J.R., Gomez, N., Hoggard, M.J., Clark, P.U., 2021. Rapid postglacial rebound amplifies global sea level rise following West Antarctic Ice Sheet collapse. Sci. Adv. 7 (18), eabf7787. https://doi.org/10.1126/sciadv.abf7787.

Pedersen, V.K., Egholm, D.L., Nielsen, S.B., 2010. Alpine glacial topography and the rate of rock column uplift: a global perspective. Geomorphology 122 (1–2), 129–139. https://doi.org/10.1016/j.geomorph.2010.06.005.

Pedersen, V.K., Knutsen, A.R., Pallisgaard-Olesen, G., Andersen, J.L., Moucha, R., Huismans, R.S., 2021. Widespread glacial erosion on the Scandinavian passive margin. Geology. 49, 1004–1008. https://doi.org/10.1130/G48836.1.

Petersen, K.D., Nielsen, S.B., Clausen, O.R., Stephenson, R., Gerya, T., 2010. Small-Scale Mantle Convection Produces Stratigraphic Sequences in Sedimentary Basins. Science (1979) 329, 827–830. https://doi.org/10.1126/science.1190115.

Peltier, W.R., Argus, D.F., Drummond, R., 2015. Space geodesy constrains ice age terminal deglaciation: the global ICE-6G_C (VM5a) model. J. Geophys. Res. Solid Earth 120, 450–487. https://doi.org/10.1002/2014jb011176.

Pronk, M., Hooijer, A., Eilander, D., Haag, A., de Jong, T., Vousdoukas, M., Vernimmen, R., Ledoux, H., Eleveld, M., 2024. DeltaDTM: A global coastal digital terrain model. Sci. Data 11, 273. https://doi.org/10.1038/s41597-024-03091-9.

Raymo, M., Mitrovica, J.X., 2012. Collapse of polar ice sheets during the Stage 11 interglacial. Nature 483, 453–456.

Reiners, P.W., Ehlers, T.A., Mitchell, S.G., Montgomery, D.R., 2003. Coupled spatial variations in precipitation and long-term erosion rates across the Washington Cascades. Nature 426, 645–647.

Rohling, E., Grant, K., Bolshaw, M., et al., 2009. Antarctic temperature and global sea level closely coupled over the past five glacial cycles. Nat. Geosci. 2, 500–504. https://doi.org/10.1038/ngeo557.

Rowley, D.B., 2013. Sea level: earth's dominant elevation – implications for duration and magnitudes of sea level variations. J. Geol. 121, 445–454.

Rowley, D.B., 2017. Earth's Constant Mean Elevation: implications for Long-Term Sea Level Controlled by Oceanic Lithosphere Dynamics in a Pitman World. J. Geol. 125, 141–153.

Ruetenik, G.A., Ferrier, K.L., Creveling, J.R., Fox, M., 2020. Earth Planet. Sci. Lett. 538, 116198. https://doi.org/10.1016/j.epsl.2020.116198.

Simms, A.R., Lisiecki, L., Gebbie, G., Whitehouse, P.L., Clark, J.F., 2019. Balancing the last glacial maximum (LGM) sea-level budget. Quat. Sci. Rev. 205, 143–153. https://doi.org/10.1016/j.quascirev.2018.12.018.

Smith, W.H.F., Sandwell, D.T., 1997. Global seafloor topography from satellite altimetry and ship depth soundings. Science (1979) 277, 1957–1962.

The MathWorks Inc, 2023. Signal Processing Toolbox Documentation. Massachusetts: The MathWorks Inc, Natick. https://mathworks.com/help/signal/ref/findpeaks.html.

Tierney, J.E., et al., 2020. Past climates inform our future. Science (1979) 370, eaay3701. https://doi.org/10.1126/science.aay3701.

von Blanckenburg, F., 2006. The control mechanisms of erosion and weathering at basin scale from cosmogenic nuclides in river sediment. Earth Planet. Sci. Lett. 242, 224–239. https://doi.org/10.1016/j.epsl.2005.06.030.

Willett, S.D., 1999. Orogeny and orography: the effects of erosion on the structure of mountain belts. J. Geophys. Res. 104, 28957–28981.

Whipple, K.X., 2009. The influence of climate on the tectonic evolution of mountain belts. Nat. Geosci. 2, 97–104.

Whitehouse, P.L., 2018. Glacial isostatic adjustment modelling: historical perspectives, recent advances, and future directions. Earth Surface Dynamics 6, 401–429. https://doi.org/10.5194/esurf-6-401-2018.

Yousefi, M., Wan, J., Pan, L., Gomez, N., Latychev, K., Mitrovica, J.X., et al., 2022. The influence of the solid Earth on the contribution of marine sections of the Antarctic Ice Sheet to future sea-level change. Geophys. Res. Lett. 49. https://doi.org/10.1029/2021GL097525 e2021GL097525.

Zachos, J., Pagani, M., Sloan, L., Thomas, E., Billups, K., 2001. Trends, rythms, and aberrations in global climate 65 Ma to present. Science (1979) 292, 686–693.